ACS Catalysis

Perspective

pubs.acs.org/acscatalysis

Cobalt-Oxide-Based Materials as Water Oxidation Catalyst: Recent Progress and Challenges

Xiaohui Deng and Harun Tüysüz*

Max-Planck Institut für Kohlenforschung, Kaiser-Wilhelm-Platz 1, D-45470 Mülheim an der Ruhr, Germany

ABSTRACT: Inspired by natural processes, there is an enormous interest in light-driven water splitting to convert solar energy into electrical and chemical energy. This approach is thought to be able to eventually solve the main energy problem that society will face more dramatically in the near future. The water oxidation reaction is widely considered a major barrier for utilizing solar energy in artificial photosynthesis. Due to the relatively high overpotential and slow kinetics of the reaction, numerous efforts are made on the development of non-noble metal oxygen evolution catalysts such as transition metal oxides. Among them, cobalt-oxide-based materials have shown decent activity and thus present themselves as a promising candidate. In this perspective, we summarize the state of the art in synthesis of cobalt-oxide-based materials and application as water oxidation catalysts through electrochemical, photochemical, and photoelectrochemical approaches. Additionally, we state the future challenges that are critical to overcome to push the catalyst performance one step further.

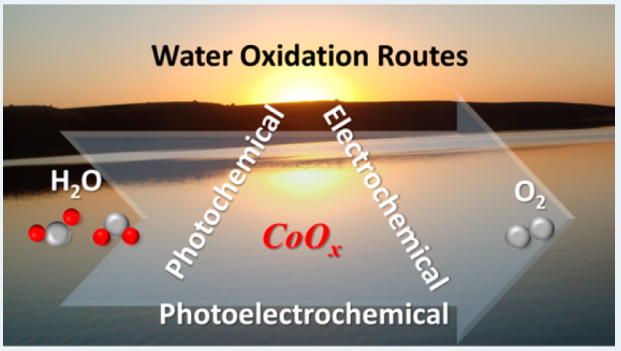

KEYWORDS: *water oxidation, cobalt oxide, electrocatalysis, photochemical/photoelectrochemical water splitting, cocatalyst*

INTRODUCTION

There has been an increasing demand for sustainable clean energy due to the shortage of fossil fuels and arising environmental issues in the last decades. The current world energy consumption is around 15 TW, and many methodologies and technologies are being suggested as possible solutions for the energy and climate problems associated with the growth of human population to around 10 billion and the corresponding energy consumption to 20 TW.[1] Solar energy is the most abundant clean energy source available with 120 000 TW of light striking the surface of the earth. Among all the efforts that have been undertaken, solar fuel production through artificial photosynthesis is emerging as an attractive approach to tackle energy problems because the solar energy can be transferred to chemical energy and stored as high energy carriers.[2−8]

Nature harvests solar energy to extract electrons and release protons from water, a process that is called photosynthetic water oxidation or oxygen evolution. This reaction is vital to the planet because it directly produces dioxygen and reducing equivalents and intermediates for carbon dioxide reduction to carbohydrates. In artificial photosynthesis schemes, either splitting water to hydrogen and oxygen or transforming carbon dioxide directly to liquid fuel, electrons must be transferred from water to the final products, in which process water is oxidized through transfer of four electrons.[9,10] Overall, water splitting consists of water oxidation and reduction as half reactions and in principle can be studied separately. Among both reactions, water oxidation is considered to be more challenging since it requires the transfer of four electrons and the formation of oxygen−oxygen bands. A large overpotential (η), which is the extra potential needed to be applied beyond the thermodynamically required value, is always mandatory for fuel production due to the relatively slow kinetics of the oxygen evolution reaction (OER). One of the major aspects to be considered for improving the overall kinetics of the OER is the nature of the electrode, which should meet the requirements such as moderate efficiency, corrosion resistance, long-term stability, and low fabrication cost. The development of stable water oxidation catalysts (WOC) with a moderate reaction rate and small overpotential still remains a challenge for the community.

Metal oxides have been intensively studied as water oxidation catalysts since they show attractive durability and activity. Oxides of noble metals, in particular RuO_2 and IrO_2, have been proven to be highly active OER catalysts with overpotentials around 300 mV to reach a current density of 10 mA/cm^2.[11−15] Although plenty of work has been conducted on the structural engineering of electrode materials, their practical application in large scales is still hindered by the scarcity and high cost of corresponding metal species. On the other hand, oxides/hydroxides of first-row transition metals have been substantially investigated as potential OER catalysts, and some of them are showing competitive catalytic performance.[16] For instance,

Received: May 25, 2014
Revised: September 4, 2014
Published: September 7, 2014

   dx.doi.org/10.1021/cs500713d | ACS Catal. 2014, 4, 3701−3714

nanostructured Mn(III) oxide has been electrochemically deposited on glassy carbon electrodes, and the obtained film demonstrates OER activity comparable to the best-known precious metal catalysts.[17] Subsequently, manganese oxide clusters supported on mesoporous silica were also shown to be able to efficiently evolve O_2 from aqueous solution through a photochemical approach.[18,19] Very recently, oxyhydroxide species such as amorphous FeOOH and NiOOH functionalized as promising WOCs in photoelectrochemical systems, where a photocurrent of 2.73 mA/cm^2 was achieved with an applied bias of 0.6 V vs RHE on porous $BiVO_4$ electrodes.[20−22] Another demonstration on transition metal oxides is the Ni−Fe hydroxide nanoplate, which was shown to be a highly active oxygen evolution catalyst in alkaline condition.[23]

Among all candidates, cobalt-based materials demonstrate decent activity and have gained considerable attention as water oxidation catalysts.[9,19,24−27] A well-known cobalt phosphate (Co−Pi) system was reported by the Nocera group in 2008, where they observed an in situ electrochemical formation of OER catalyst on ITO substrate from a phosphate-buffered solution containing Co^{2+} ions.[28−30] The formed catalyst layer was able to oxidize water under a neutral pH with a moderate overpotential. Following this, the electrolyte influence, such as the buffer solution species and Co^{2+} concentration, were investigated, and the analogous cobalt borate system was applied in a practical manner to silicon-based light-harvesting semiconductors.[31,32] In order to further understand the reaction mechanisms, X-ray spectroscopy and electron paramagnetic resonance measurements were employed, and the presence of Co(IV) was proposed to be responsible for the water oxidation at neutral pH.[33,34] Molecular $[Co_4(H_2O)_2(PW_9O_{34})_2]_{10}-$ (Co_4−POM) was also reported as active water oxidation catalyst with a catalytic turnover frequencies above 5 s^{-1} at pH 8, although the identification concerning the true catalyst (CoO_x or Co_4−POM) under reaction conditions still remains a challenge.[35−37] Apart from these achievements, a vast amount of work has been conducted on cobalt oxide (CoO_x)-based materials, and promising results have been shown for oxidation evolution through electrochemical, photochemical, and also photoelectrochemical approaches.[38−41] In this perspective, we will briefly discuss the recent progress concerning the materials design and synthesis in this specific field and at the end give a brief outlook.

ELECTROCHEMICAL WATER OXIDATION BY COBALT-OXIDE-BASED CATALYSTS

Electrochemical water splitting or electrolysis of water is a process where water molecules are decomposed into oxygen and hydrogen under applied external bias (electric voltage). As shown in Figure 1, in a typical electrochemical cell, an electrical power source is connected to the anode and cathode, where the oxidation and reduction reactions occur, respectively. Electrolysis of water needs excess energy in the form of overpotential to overcome the activation barriers. Although this process produces clean hydrogen, it is barely used in industrial applications because hydrogen production through steam reforming of fossil fuels is more affordable. As a result of the shortage of the fossil fuels and their harsh effects on the environment, currently there is a massive interest in water electrolysis to produce clean hydrogen. With respect to the practical and economical aspects, it is essential to develop cheaper and more efficient catalysts.

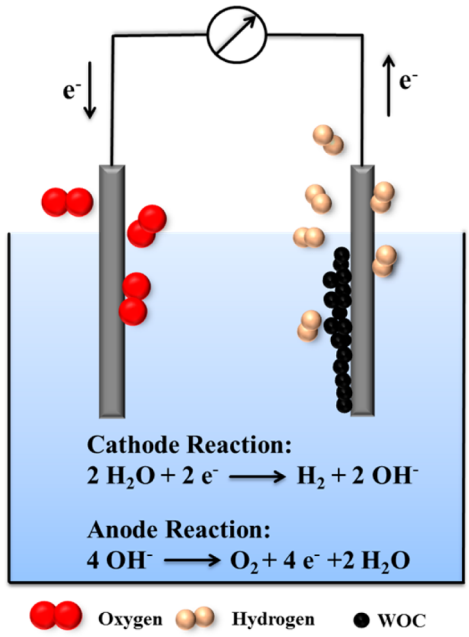

Figure 1. Schematic description of electrolysis of water.

In order to gain a reasonable evaluation for the electrocatalytic activity of water oxidation catalysts in lab scales, three-electrode systems with a rotating disc electrode configuration are generally employed. Usually, an alkaline electrolyte is used for transition metal oxide catalysts in order to increase the conductivity of electrolyte and inhibit the oxide corrosion, which is the major issue under acidic working condition. The rotation of the electrode is critical to remove the gaseous product and thus avoid bubble accumulation on the electrode surface. To check the activity, a polarization scan or cyclic voltammogram is conducted at reasonable scan rates, typically 20−50 mV/s. Because a current density of 10 mA/cm^2 is expected for an integrated solar water splitting device with 10% solar-to-fuel efficiency, the overpotential required to reach this value is in general a key parameter to assess an oxygen evolution catalyst.[17,42] Another practical issue concerning electrocatalysts is material stability. This can be characterized either by controlled-current electrolysis, where the voltage required to obtain a certain value of current is recorded, or by chronoamperometric measurement, where the current at a constant applied voltage is recorded during an appropriate time period under working conditions. Other details concerning the evaluation of electrochemically surface area, Faradaic efficiency, and turnover frequency (TOF) can be found in a comprehensive protocol recently described by the Jaramillo group.[42]

Co_3O_4 has a spinel structure, which consists of Co^{2+} at the tetrahedral sites and Co^{3+} at the octahedral sites. The change of surface species of cobalt oxide spinel upon base conditions has been studied by cyclic voltammetry intensively since the late nineties by electrochemists.[43−46] It is widely agreed that at the rest potential, the surface of Co_3O_4 is partially oxidized to a CoOOH phase, and with further increasing the applied voltage, an anodic feature appears before the onset of water oxidation reaction, which is attributed to the CoO_2/CoOOH redox couple.[47] These findings suggested that the presence of Co^{IV} may be essential to catalyze oxygen evolution, and this view is further supported by recent experimental work, where gold

dx.doi.org/10.1021/cs500713d | ACS Catal. 2014, 4, 3701−3714

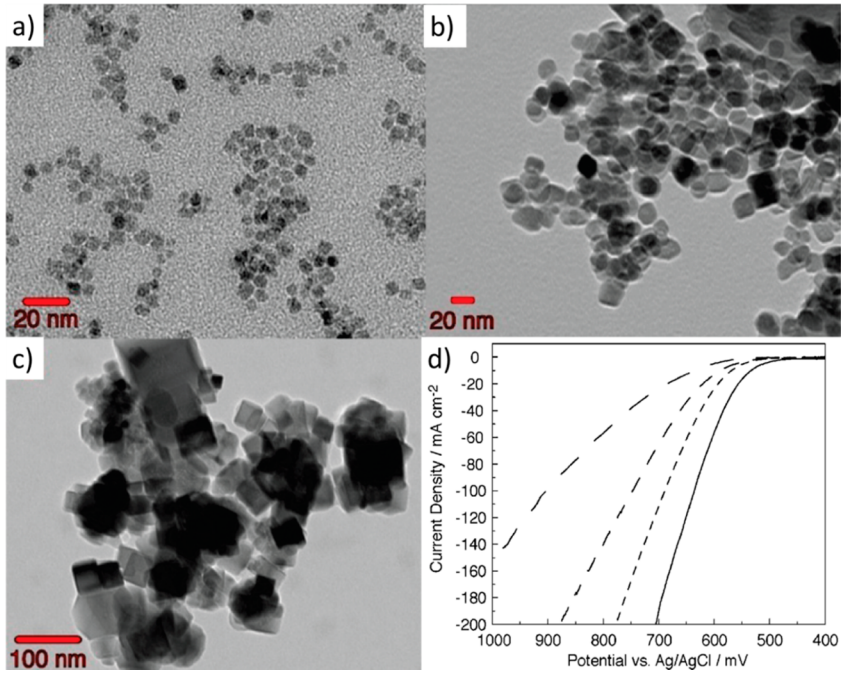

Figure 2. TEM images of cubic Co_3O_4 nanoparticles with average sizes of (a) 6, (b) 21, (c) 47 nm. (d) Polarization activities for Co_3O_4 nanoparticles loaded Ni foam in 1.0 M KOH electrolyte. Scan rate: 1 mV/s. Ni foam area: 1 cm^2. Catalyst loading: 1 mg/cm^2. Reprinted with permission from ref 59. Copyright 2009 American Chemical Society.

supports or nanoparticles have been proven to enhance the water oxidation activity of cobalt oxide by increasing the population of Co^{IV} due to the electronegativity of gold.[48,49] Discussion of the details concerning the water oxidation mechanism on Co oxide surface can be found elsewhere.[50,51]

Nevertheless, the development of nanotechnology has enabled us to synthesize materials with unique mechanical, electrical, and optical properties compared with bulk materials.[52−54] By tuning the size and nanostructure, superior catalytic performance compared with traditional bulk materials can be achieved.[55−57] High surface area is especially favored in catalysis due to the fact that more active sites would be present on the surface. Because the catalytic reaction happens on the surface atoms, the surface-to-volume ratio is a critical parameter in heterogeneous catalysis. A particle with 100 nm size has around 1% surface atoms, whereas particles with 10 and 1 nm size have about 10% and 90% surface atoms, respectively. Syntheses of cobalt-based nanoparticles have been well developed, and the particle size can be precisely controlled by adjusting the reaction conditions. For example, in the hydrothermal approach proposed by Zhang, particles with average sizes of 3.5, 6, 11, 19, and 70 nm were prepared by varying the solvent composition and the cobalt precursor amount.[58] OER activity of Co_3O_4 nanoparticles with various sizes were further investigated by Bell and Tilley, where they loaded nanoparticles in size of 6, 21, and 47 nm on Ni foam and evaluated their catalytic activity for oxygen evolution from 1.0 M KOH electrolyte.[59] It was found quantitatively that the increase in surface area by 1 order of magnitude decreased the overpotential by 50 mV at a fixed current density of 10 mA/cm^2, as shown in Figure 2. Later on, the comparison of cobalt-based nanoparticles with different oxidation state and crystal structure—Co_3O_4, CoO, and ε-Co in size of ∼10 nm—was reported by the same group, where very similar catalytic activities were observed after 20 consecutive scans under basic conditions. It was attributed to the similar particle size, surface species, and reaction mechanisms.[60]

Apart from traditional synthesis routes, very recently a PLAL (Pulsed-Laser Ablation in Liquids) method was developed, and it was able to prepare surfactant-free Co_3O_4 nanoparticles with a size of ∼2.5 nm.[61] The crystalline material showed an overpotential of 314 mV at 0.5 mA/cm^2 in 1 M KOH. Moreover, cobalt oxide nanoparticle/carbon composites have proven themselves to be an approach to push the performance of water oxidation electrocatalysts one step further. Two-dimensional graphene/graphene oxide has been explored in numerous applications for energy storage and conversion due to the advantages such as high conductivity, charge carrier mobility, high surface area, and outstanding durability compared with other carbon materials.[62−67] Through a facile hydrothermal approach, Co_3O_4 nanocrystals were grown on mildly oxidized graphene oxide sheets.[68] The size of nanocrystals was further reduced from 15 to 25 nm to 4−8 nm by adding NH_4OH during the synthesis, which introduced an interaction between NH_3 and cobalt cations. In 1 M KOH solution, the hybrid material showed a rather stable electrocatalytic activity with overpotential of ∼330 mV at 10 mA/cm^2, being among the best nonprecious metal-based catalysts for oxygen evolution. Co_3O_4/SWNTs (single-walled carbon nanotubes) hybrid materials were demonstrated later by the Xie group, where a superior OER activity compared with bare Co_3O_4 was observed in neutral and alkaline solution.[69] Overall, the unusual catalytic activity of such materials arises from synergetic chemical and electric coupling effects between active nanocrystals and carbon supports.

Besides nanoparticles, mesoporous metal oxides are another category of nanostructured materials that are particularly attractive for heterogeneous catalysis. Mesoporous materials refer to solids with distribution of pores in the size range of 2 to 50 nm. In the past decades, multiple efforts have been made on

dx.doi.org/10.1021/cs500713d | ACS Catal. 2014, 4, 3701−3714

the syntheses of mesoporous frameworks with uniformly ordered pore systems because they combine high surface area, crystalline walls, rigid frameworks, and durable stabilities.[70−73] Among all the synthesis strategies, hard templating (nanocasting) processes were studied deeply, and a wide range of transition metal oxides have been successfully prepared.[74−76] In a typical nanocasting procedure (Figure 3), a hard template

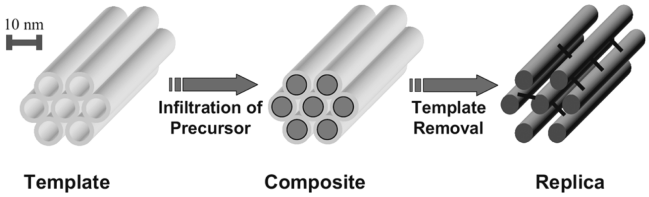

Figure 3. Schematic illustration of nanocasting pathway. Reprinted with permission from ref 74. Copyright 2006 Wiley-VCH Verlag GmbH & Co. KGaA, Weinheim.

(mostly ordered mesoporous silica) is first prepared. In the second step, the template is impregnated with suitable precursors and followed by calcination under air or inert atmosphere. In the final step, the silica template is removed with hot alkaline solution and the products result in an inverse replica of the hard template. By varying the precursor, the type, and the texture parameters of the hard template, one can easily control the dimension, symmetry, domain and crystallite size, texture parameters, and crystallinity of the final products.[77−79]

This class of materials offers many fascinating properties and a range of catalytic functions, as illustrated in Figure 4.

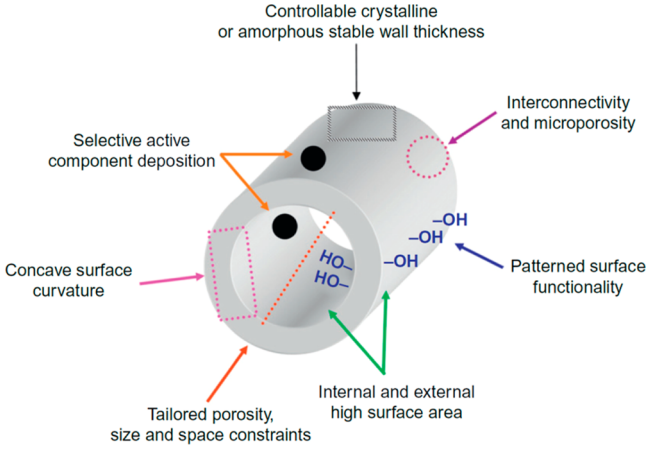

Figure 4. Properties of ordered mesoporous oxides those are responsible for exceptional catalytic performance. Reprinted with permission from ref 72. Copyright 2013 Elsevier Books.

Properties such as composition, crystallinity, thermal/chemical stability, surface area, porosity, surface curvature, and surface functionality (which can also be provided by anchored active sites) have effects on the catalytic activity of ordered mesoporous metal oxides (OMMs).[72] The main advantages that differentiate these materials from many others as catalysts are the high surface area, the tunable porosity and composition, and the structural stability.

In the past few years, our group has devoted considerable effort to the design of various ordered mesoporous materials, in particular for magnetic and catalytic applications.[55,80−90] Based on the idea of utilizing ordered mesoporous transition metal oxides for the water oxidation reaction due to their distinctive physical and chemical properties, our group focuses on ordered mesoporous Co_3O_4. As the basis of our study, pure Co_3O_4 was first prepared using cubic ordered mesoporous silica as a hard template via the nanocasting route.[91] As aforementioned, by controlling the aging temperature during the hydrothermal synthesis of the silica hard template, the pore size, crystallite size, symmetry, and more interestingly, the surface area of Co_3O_4 replica was tuned. As shown in the TEM images (Figure 5), Co_3O_4-35, which was fabricated from KIT-6—a widely used ordered mesoporous silica template with cubic symmetry—aged at the temperature of 35 °C, has a more open, uncoupled subframework compared with Co_3O_4-100 and Co_3O_4-135 (100 and 135 indicate aging temperature of KIT-6 silica hard template).

In addition, the pore size of the silica hard template increases with higher aging temperature. Consequently, the particle size and surface area of the Co_3O_4 replica originating from such templates would follow an opposite trend. This was well supported by N_2 sorption measurements where surface areas of 156, 113, and 72 m^2/g for mesoporous Co_3O_4 were obtained. Then, the electrocatalytic activities of nanocast Co_3O_4 were investigated in alkaline condition, and the catalytic performance was found to be significantly dependent on the external surface area. The highest activity was achieved on Co_3O_4-35, which had the highest surface area due to the higher number of the catalytic sites on the surface. The structural stability and catalytic durability were tested by applying a constant bias at 0.8 V vs Ag/AgCl at pH 13, and it was found that the measured current density did not show visible deactivation in 100 min, with the mesoporous framework of the catalyst remaining intact. Similar work on mesoporous Co_3O_4 for water oxidation electrocatalysts was also conducted by the Joo group.[92]

It is important to compare the ordered mesoporous structures with the analogous nonordered structures and nanoparticle morphology in order to identify the advantages of such nanostructure. Thus, we recently synthesized Co_3O_4 nanoparticles, mesoporous Co_3O_4 from a disordered mesoporous silica-gel template, Co_3O_4 in bulk form, and further tested in electrochemical water oxidation. From the linear sweeps presented in Figure 6, it can be seen that the Co_3O_4 with ordered mesoporous structure clearly indicates higher catalytic activity than disordered Co_3O_4 templated from silica gel and nanoparticle counterparts. The bulk Co_3O_4 shows the lowest activity due to the lowest surface area. A distinct advantage of mesoporous Co_3O_4 over nanoparticle is that the skeleton can be quite stable during the storage and harsh reaction conditions while the nanoparticles tend to aggregate. This results in larger size which consequently lowers the number of catalytic active sites.[38]

Composite or alloy materials have been shown to be superior catalysts in various applications.[93−95] Taking ordered mesoporous Co_3O_4 as a skeleton material, we further fabricated a family of composite materials based on a solid−solid reaction of Co_3O_4 with other transition metal oxides.[38] In detail, the porous Co_3O_4 template was first filled with metal precursor by a wet-impregnation route. After drying, the mixture was then thermally decomposed at relatively low temperature (250 °C) to form a reactive dopant oxide species on the cobalt oxide surface. Final calcination at 550 °C promoted the reaction between metal oxide and Co_3O_4, resulting in a composite phase. N_2 sorption measurements along with electron microscopy showed that the typical mesoporous structures

dx.doi.org/10.1021/cs500713d | ACS Catal. 2014, 4, 3701−3714

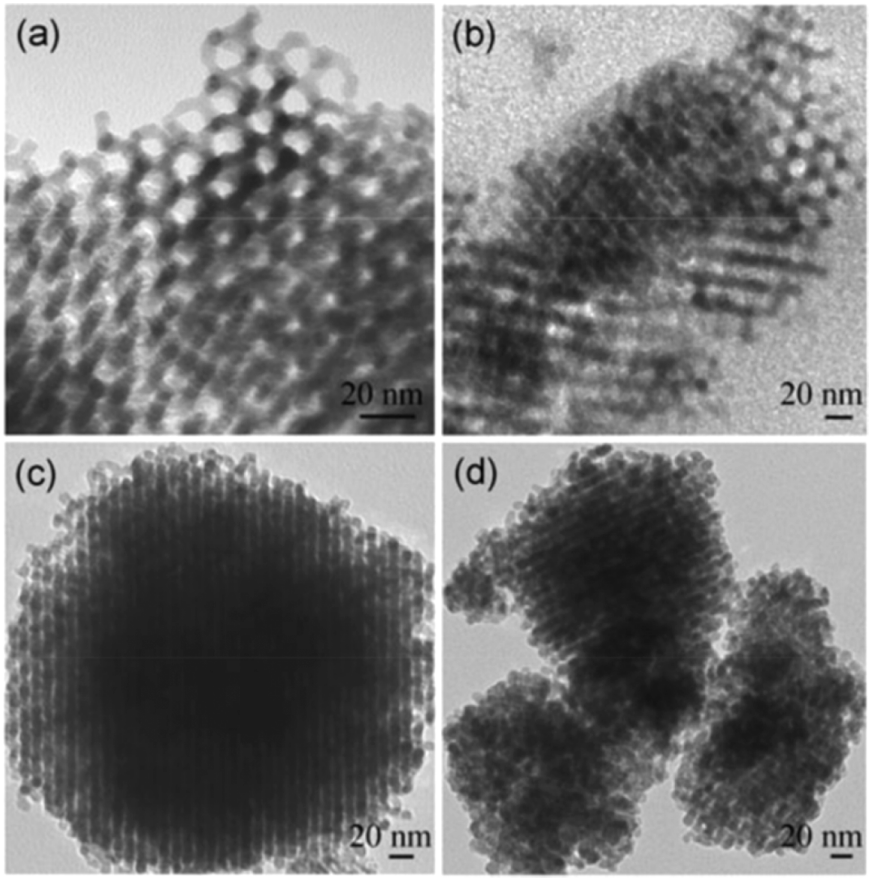

Figure 5. TEM images Co_3O_4-35 (a), Co_3O_4-100 (c), Co_3O_4-130 (d), and Co_3O_4-35 after electrochemical measurement (b). Reprinted with permission from ref 91. Copyright 2014 Springer.

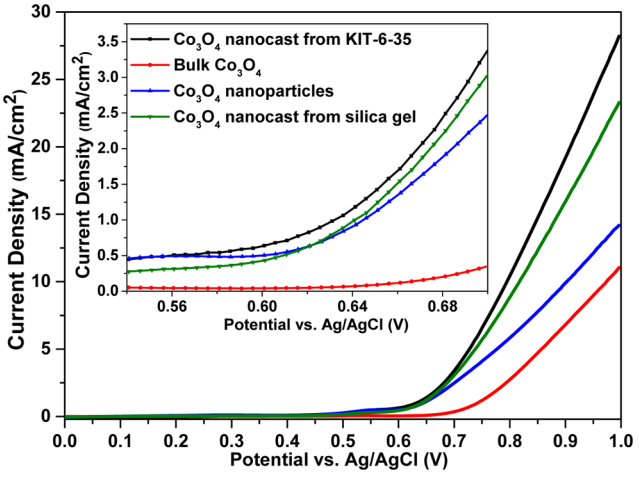

Figure 6. Comparison of Co_3O_4 with various morphologies as electrochemical water oxidation catalysts. For experimental, catalysts were dispersed on glassy carbon electrode and measured in 0.1 M KOH electrolyte (catalyst loading ~0.12 mg/cm^2 for all the samples). The inset figure shows the current increment in a narrow voltage range (0.54−0.70 V vs Ag/AgCl). Adapted with permission from ref 38.

were retained after the thermal treatment. Overall, this versatile strategy allows the preparation of composite materials with similar morphology and textural parameters but with diverse surface species of mixed transition metal oxides, which can be of great interest in catalysis.

Catalytic activities of prepared composite materials were investigated for water oxidation reaction in alkaline conditions. It was found that the nanocast Co_3O_4 doped with Fe, W, Mo, and Ni showed comparable catalytic behavior as pure Co_3O_4, though the current densities were slightly different at higher applied voltages. On the other hand, Co_3O_4−$CuCo_2O_4$ showed a significantly lower onset potential for water oxidation and a higher current density in spite of the lower BET surface area in comparison with ordered mesoporous Co_3O_4. The enhancement is more remarkable in a narrow overpotential range, as shown in Figure 7a. Inspired by the Cu surface-doped Co_3O_4, a series of samples with different amounts of Cu were prepared by the direct nanocasting method, in which Cu was homogeneously distributed in the catalyst by impregnating Co and Cu precursors simultaneously. The polarization curves are shown in Figure 7b. As can be seen, higher OER activity from the homogeneously doped material was observed compared with the surface doped one. The enhancement could be attributed to the relatively higher surface area due to the fact that the mesoporous structure was partially disturbed by the surface modification methodology. In a specific case of $Cu_xCo_yO_4$ (y/x = 8), current density of 10 mA/cm^2 was obtained with an overpotential of 391 mV in 1 M KOH solution, which is quite comparable to the benchmarking OER electrocatalyst proposed by Jaramillo group recently.

Another interesting example we recently demonstrated is Fe incorporated mesoporous Co_3O_4.[41] Although there is common agreement that the symmetry of the replica obtained from cubic ordered mesoporous KIT-6 template is dependent on the

dx.doi.org/10.1021/cs500713d | ACS Catal. 2014, 4, 3701−3714

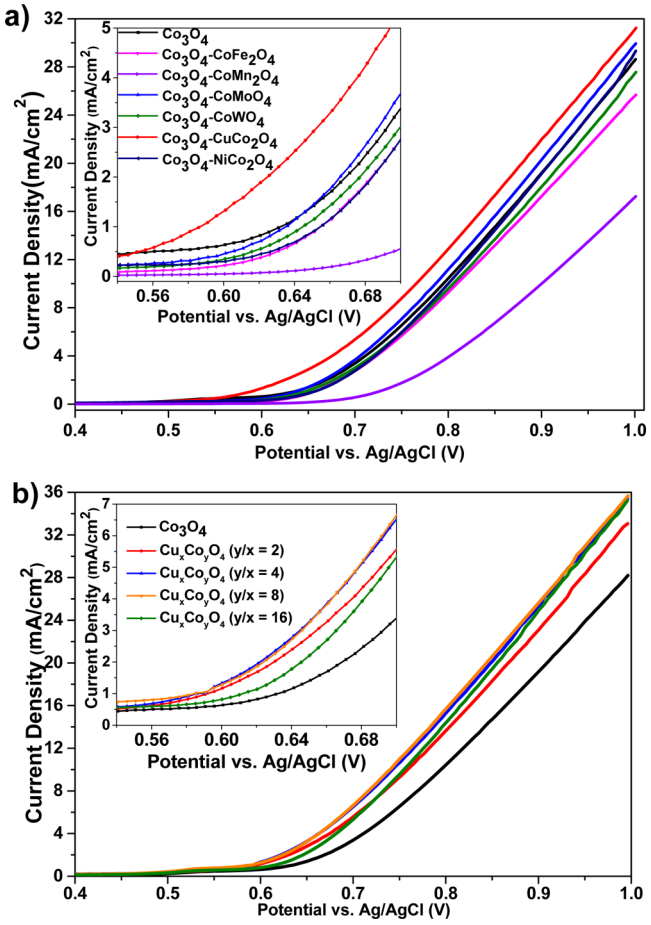

Figure 7. Oxygen evolution currents of (a) as-made Co_3O_4, Co_3O_4–CoM_2O_4 (M = Fe, Mn), Co_3O_4–$CoMO_4$ (M = Mo, W), and Co_3O_4–MCo_2O_4 (M = Cu, Ni) composites and (b) of as-made mesoporous Co_3O_4, $Cu_xCo_yO_4$ (y/x = 2, 4, 8, 16) samples. Catalysts were dispersed on glassy carbon electrode and measured in 0.1 M KOH electrolyte (catalyst loading ~0.12 mg/cm^2 for all the samples). The inset figure shows the current increment in a narrow voltage range (0.54–0.70 V vs Ag/AgCl). Adapted with permission from ref 38.

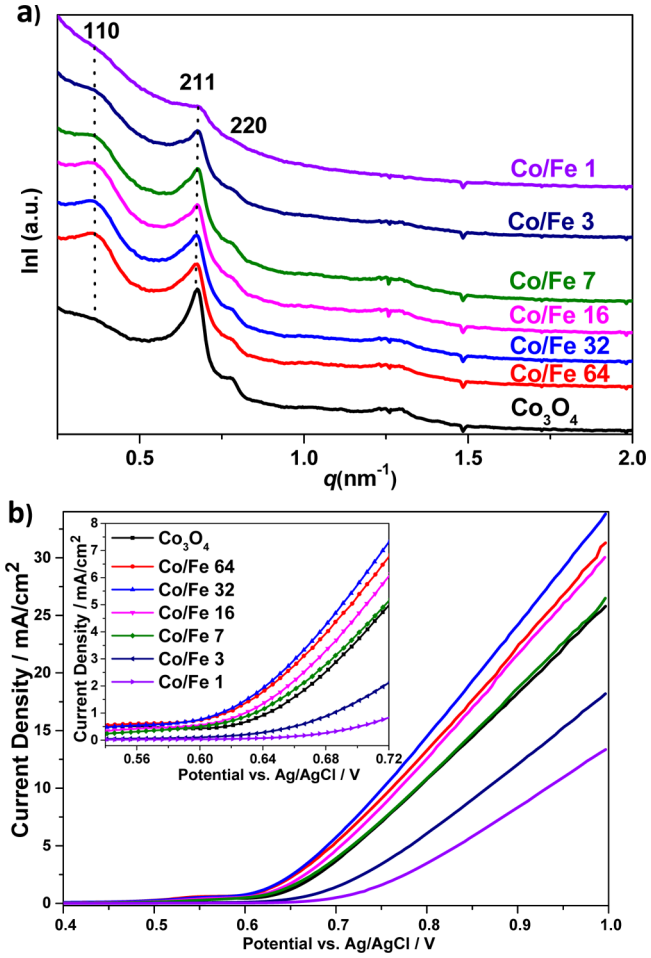

Figure 8. SAXS profile Co_3O_4 and Fe–Co_3O_4 with various iron amounts (a). Oxygen evolution currents of ordered mesoporous Co_3O_4 and Fe–Co_3O_4 with various iron amounts (b). Catalysts were dispersed on glassy carbon electrode and measured in 0.1 M KOH electrolyte (catalyst loading ~0.12 mg/cm^2 for all the samples). The inset figure shows the current increment in a narrow voltage range (0.56–0.72 V vs Ag/AgCl). Reprinted with permission from ref 41.

interconnectivity between both channels in the nanocasting process, we found that the symmetry and mesoporous structure of Co_3O_4 can be further tuned by a small amount of Fe doping.[96,97] As shown in the SAXS (small angle X-ray scattering) profile (Figure 8a), pure nanocast Co_3O_4 shows a typical pattern with (211) and (220) reflections, which has the symmetry of $Ia\bar{3}$ d as one would expect from a KIT-6 template aged at 100 °C. However, when Fe precursor was added in the impregnation procedure—even at Co/Fe atomic ratio of 64—the obtained replica indicated an extra (110) reflection, which was assigned to a lower symmetry of $I4_132$.[98] Furthermore, iron-doped Co_3O_4 samples with an atomic ratio of 64, 32, 16 (Co/Fe) showed enhanced OER activities than pure Co_3O_4 (Figure 8b), and we assume this to be related with the textural parameters, crystal, and/or electronic structures of materials.

Besides crystalline nanostructured materials, progress was also made on the preparation of amorphous cobalt oxide for catalyzing OER reaction. For instance, electrodeposition of CoO_x, $NiCoO_x$, $CoFeO_x$ has been achieved by early researchers while recently a comprehensive survey on catalytic activity toward water oxidation was performed.[42,99,100] These non-noble metal catalysts all showed similar but promising activity in 1 M NaOH electrolyte, reaching a current density of 10 mA/cm^2 in an overpotential range between 0.35 and 0.43 V. It was found that under alkaline conditions, cobalt-oxide-based OER catalyst showed superior stability compared with electrodeposited IrO_x during 2 h of constant current electrolysis, although a lower overpotential of ~0.32 V was observed at the initial period for the latter. However, the electrodeposition technique does not translate to every metal, and the composition of the deposited film is not convenient to control due to the specific voltage response of metal species.

Aiming on this goal, another new methodology, which is named as photochemical metal–organic deposition (PMOD), is reported to be a facile technique to deposit amorphous metal oxide with precise control of compositions.[101] In this approach, solutions of metal precursor complexes were first prepared by dissolving desired amounts of precursors in hexane. Then the solution was deposited on a conductive substrate (fluorine doped tin oxide (FTO)) by spin coating and irradiated with UV light to liberate the low molecular weight ligands from metal. Annealing at 100 °C completed the film preparation. This particular methodology allows the synthesis of amorphous metal oxide films in complex compositions with homogeneous

dx.doi.org/10.1021/cs500713d | ACS Catal. 2014, 4, 3701–3714

Table 1. Preparation, Electrochemical Test Condition, and Performance of Representative Metal Oxide Electrocatalysts for Water Oxidation

materials	synthesis method	sample amount/electrode/ electrolyte (if available)	Tafel slope (mV/dec)	overpotential (mV) at 10 mA/cm^2	ref
IrO_x	photochemical metal−organic deposition (PMOD)	0.1 μg cm^{-2}/FTO/1 M H_2SO_4	∼34	220	14
IrO_x	electrodeposition	glassy carbon (GC) /1 M NaOH		320	42
Ni−Fe LDH(layered double hydroxide)/CNTs	hydrolysis and solvothermal treatment	0.2 mg cm^{-2}/GC/0.1 M NaOH	∼31	300	23
MnO_x	electrodeposition	GC/0.1 MNaOH		440	17
NiO_x	electrodeposition	GC/1 M NaOH		420	42
$NiCoO_x$	electrodeposition	GC/1 M NaOH		380	42
$NiCuO_x$	electrodeposition	GC/1 M NaOH		410	42
CoO_x	electrodeposition	GC/1 M NaOH		390	42
$CoFeO_x$	electrodeposition	GC/1 M NaOH		370	42
CoO_x	photochemical metal−organic deposition (PMOD)	FTO/0.1 M KOH	∼42		101
$Fe_{40}Co_{40}Ni_{20}O_x$	PMOD	FTO/0.1 M KOH	∼31		101
Co_3O_4 NPs (∼5.9 nm)	hydrothermal	1 mg cm^{-2}/Ni foam/1 M KOH		328	59
CoO NPs (∼10 nm)	organic synthesis	1 mg cm^{-2}/Ni foam/1 M KOH		291	60
Co_3O_4 nanocrystals/*N*-graphene	hydrothermal	0.24 mg cm^{-2}/GC/0.1 M KOH	∼67	310	68
Co_3O_4 NPs/CNTs	noncovalent functionalization	0.05 mg/ITO/ 0.1 M phosphate buffer	∼104		69
meso-Co_3O_4	nanocasting	0.12 mg cm^{-2}/GC/0.1 M KOH		525	91
Fe-doped *meso*-Co_3O_4	nanocasting	0.12 mg cm^{-2}/GC/0.1 M KOH		486	41
meso-$Cu_xCo_yO_4$	nanocasting	0.12 mg cm^{-2}/GC/1 M KOH		391	38
meso-Co_3O_4 with Au NPs	nanocasting	∼0.015 mg/GC/0.1 M NaOH	∼46	440	49

distribution of metal species. Fe_2O_3, CoO_x, NiO_x, and $Fe_xCo_yNi_zO$ were prepared by PMOD and the cobalt-based materials showed outstanding activity for oxygen evolution. In the case of $Fe_xCo_yNi_zO$, a detailed study was conducted to investigate the effect of concentrations of specific metals.[102] It was found that an appropriate addition of Fe would produce an improvement in overpotential and Tafel slope while the presence of Ni and Co was critical for lowering the potential at which the reaction initiated. Both factors made the ternary amorphous $Fe_{40}Co_{40}Ni_{20}O_x$ a comparable OER catalyst to noble metal oxides.

Above-mentioned water oxidation electrocatalysts are summarized in Table 1, where experimental details (sample weight, support, and electrolyte) are listed as well, because the material performance is closely related to the practical conditions. Although some of the information is missing from the reports due to various criteria, the materials represent the benchmark for cobalt-oxide-based electrocatalyst. It should be kept in mind the value of the overpotential at a certain current density depends on several parameters including the electrochemical setup, type and concentration of the electrolyte, film preparation method, sample amount, and so forth.

PHOTOCHEMICAL WATER OXIDATION BY COBALT-OXIDE-BASED CATALYSTS

In addition to electrocatalytic water oxidation, cobalt-oxide-based materials were also utilized in photocatalytic water oxidation, where a $[Ru(bpy)_3]^{2+}$-$Na_2S_2O_8$ system was well established and the Ru species was employed as a sensitizer to harvest the light.[103,104] As illustrated in Figure 9, in a typical reaction scheme, $[Ru(bpy)_3]^{2+}$ as a sensitizer is first excited by light irradiation. The electron is then transferred to $S_2O_8^{2-}$ and thus generating a oxidized $[Ru(bpy)_3]^{3+}$ species. The oxidation of water happens upon the collision between water oxidation catalyst (WOC) and $[Ru(bpy)_3]^{3+}$, where the hole is injected to

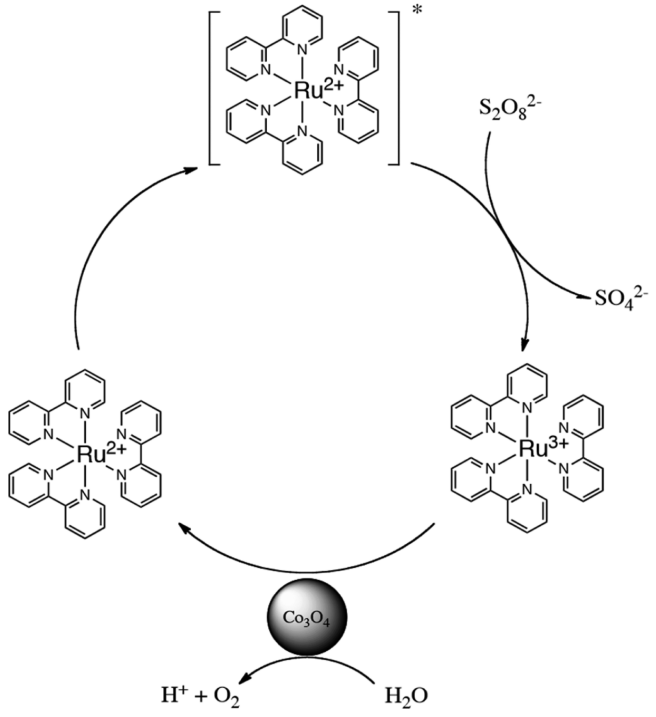

Figure 9. Schematic illustration of visible light sensitization of Co_3O_4 WOC by excitation of $[Ru(bpy)_3]^{2+}$ in the presence of $S_2O_8^{2-}$. Adapted with permission from ref 107. Copyright 2014 Macmillan Publishers Limited.

the WOC. The overpotential for water oxidation generated using this system is 350 mV at the pH value of 5.8.[18] The hole injection process can be further directed by connecting oxygen evolving catalyst with hole conducting molecular wires.[105,106] Experimentally, the detection of evolved O_2 from WOC is done using a Clark electrode at short time scales and a reactor-mass

dx.doi.org/10.1021/cs500713d | ACS Catal. 2014, 4, 3701−3714

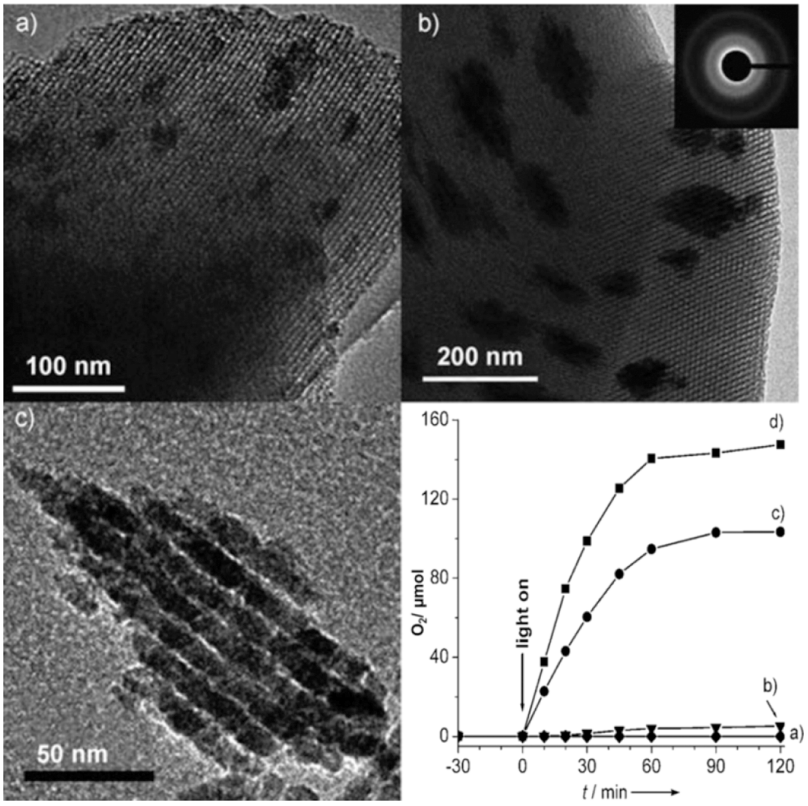

Figure 10. TEM images of (a) SBA-15/Co_3O_4 (4%), (b) SBA-15/Co_3O_4 (8%), and (c) Co_3O_4 (8% sample) after removal of SBA-15 substrate using hot NaOH solution. (d) Oxygen evolution in aqueous suspensions (40 mL) of (a) SBA-15/NiO (8%), (b) micron size Co_3O_4 particles, (c) SBA-15/Co_3O_4 (8%), and (d) SBA-15/Co_3O_4 (4%). Adapted with permission from ref 24. Copyright 2009 Wiley-VCH Verlag GmbH & Co. KGaA, Weinheim.

spectrometer (in some cases, a gas chromatograph) setup in a long time period. A Clark electrode system consists of a semipermeable membrane which allows the diffusion of oxygen, an Ag/AgCl anode which provides electrons for O_2 reduction and a noble metal cathode where O_2 is reduced. Because the oxygen which passes through the membrane is reduced in the cathodic reaction, the electrode produces a current at a constant polarizing voltage, and the amplitude of the current is dependent on the partial pressure of diffused oxygen. In this way, the amount of O_2 dissolved in the overall solution is calculated.[19,107] This method is very powerful to investigate the initial catalysis behavior of the WOC, because it has been suggested that on a relatively short time scale, the initial surface species are critical for catalysis even if the catalyst itself is not stable.[40] However, because the surface of the catalyst will undergo reconstructing under catalytic environment and the reaction mechanism can differentiate from each other on different active sites, the investigation of long-term catalysis behavior and stability is essential for material evaluation.[40,107] To achieve this purpose, the reactor is combined with mass spectroscopy (MS) and gas chromatography (GC), and the gas phase in the head space can be analyzed. It is worth noting that the amount of oxygen dissolved in solution should also be taken into account.

One system that has been intensively investigated in photocatalytic water oxidation is cobalt oxide clusters supported on mesoporous silica scaffolds.[18,19,24] The composite material was synthesized by wet impregnation of cobalt precursor into ordered mesoporous SBA-15 silica followed by calcination. As shown in Figure 10a,b, uniform distribution of cobalt oxide nanoclusters was obtained on hexagonally ordered mesoporous SBA-15 silica with different loading. A detailed picture of single Co_3O_4 nanocluster after silica leaching is shown in Figure 10c.

Evolution of oxygen catalyzed by Co_3O_4 nanoclusters was observed in the aforementioned $[Ru(bpy)_3]^{2+}$-$Na_2S_2O_8$ system, and a TOF of 1140 s^{-1} per Co_3O_4 nanocluster was calculated for SBA-15/Co_3O_4 with (4 wt % loading). Specifically, the TOF number here was calculated on the basis of the number of clusters (overall loading divided by the approximate weight of each cluster, while the average cluster size was determined according to TEM micrographs) applied in the catalysis and overall oxygen yield. Further increasing the catalyst loading led to a higher TOF of 3450 s^{-1} per cluster. However, due to the increasing number of nanorods per silica and less access to water, a lower TOF based on projected area was observed. To investigate the role of the silica support, the activity of SBA-15/Co_3O_4 composite was compared with bare clusters devoid of the silica scaffold and micrometer-size Co_3O_4 particles. After the removal of silica by NaOH etching, the bare clusters showed severe aggregation, and the O_2 yield per second for silica supported nanorod was 1550 times higher than micron size Co_3O_4 particles on condition that same amount of Co_3O_4 was taken into account. Figure 10d shows the oxygen evolution comparison for prepared composite materials. This enhancement was mainly attributed to the substantially large geometrical surface area provided by nanostructure. In addition, Co surface sites of nanoclusters were more catalytically efficient than those of micrometer-sized particles.[24] The effect of geometry of silica supports was further investigated by Jiao

dx.doi.org/10.1021/cs500713d | ACS Catal. 2014, 4, 3701−3714

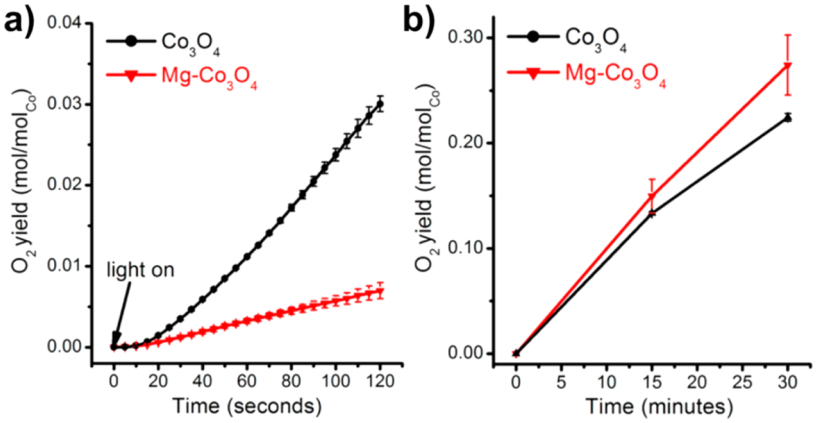

Figure 11. Oxygen yield for mesoporous Co_3O_4 and Mg-substituted Co_3O_4. Measurements were conducted in (a) Clark electrode system for 120 s and (b) reaction-GC system for 30 min. Reprinted with permission from ref 40. Copyright 2014 American Chemical Society.

group and KIT-6 with a 3D porous structure was found to be a better support than SBA-15 which has 1D parallel channels.[108] This phenomenon could be due to the more convenient reactant transport in the 3D cubic nanostructure.

Co_3O_4/mesoporous silica composite materials were also prepared by impregnating silica templates with prior-prepared Co_3O_4 nanoparticles.[109] In this case, the size of ligand-free Co_3O_4 nanoparticles was precisely controlled by synthetic strategy, and a detailed study on the size effect was conducted. Unsurprisingly, the activity toward OER increased with decreasing particle size. It is worth noting that the functionality of the silica template was to prevent nanoparticle aggregation and scatters incoming light to enhance light absorbance. The X-ray photoelectron spectroscopy (XPS) results also indicated that due to the heterojunction between Co_3O_4 nanoparticle and silica, the oxidation state of cobalt was higher than that for bulk materials, which could affect the activity for water oxidation. Independent cobalt-based spinel nanoparticles were also prepared by hydrothermal synthesis, and it has been shown that the photocatalytic water oxidation activity could be further tuned by substituting cobalt with other transition metals in the spinel structure.[110] Recent studies showed that the catalytic activity is dependent on the binding strength between metal and oxygen evolution intermediates. In the case of Mn-substituted Co_3O_4 nanoparticles which had a higher TOF (8.7×10^{-4} per transition metal) compared with Co_3O_4 nanoparticle (5.8×10^{-4} per transition metal), the oxidation state of Mn was calculated to be 3.1 and it was proposed that $Mn^{3.1+}$ at the octahedral sites of Co_3O_4 spinel had the optimal binding energy.[110] However, when the material was prepared in a mesoporous manner, the oxidation state of the introduced Mn was calculated to be 3.7. This resulted in a negative effect on the binding energy and was unfavorable for oxygen evolution compared with mesoporous Co_3O_4.[111]

A rather interesting study reported recently by the Jiao group was the fabrication of mesoporous Co_3O_4 with high surface area by the selective leaching of Mg in the spinel structure.[40] Mesoporous Mg−Co_3O_4 with an atomic ratio of Mg/Co = 0.36 was first prepared by the nanocasting method. A surface area of 102 m^2/g was obtained, and it was typical for a replica from the KIT-6 hard template (aging temperature 100 °C). The X-ray absorption spectroscopy showed that the Mg atoms were randomly distributed at both tetrahedral and octahedral sites. The initial photocatalytic water oxidation measurement was conducted in a Clark electrode system within a period of 120 s. As shown in Figure 11, pure Co_3O_4 exhibited better oxygen evolution activity than Mg-substituted counterpart. However, when the same reaction was carried out in the reactor-GC system to check the long-term catalyst behavior, the Mg-substituted Co_3O_4 showed surprisingly high activity compared to Co_3O_4, with a TOF of 1.6×10^{-3} s^{-1} per surface Co atom (the TOF for mesoporous Co_3O_4 was 5×10^{-4} s^{-1}). This enhancement was later attributed to the Mg leaching process which happened under weak acidic environment (pH = 5.8). In detail, due to the loss of Mg cations from the octahedral sites, defects or vacancies in the spinel structure were created, and the catalyst was activated. The recovered catalyst was later characterized and the Mg to Co ratio dropped to 0.27 after reaction, while the mesoporous nanostructure, oxidation state, and coordination environment of Co remained the same as original Mg−Co_3O_4. N_2 sorption measurement indicated that the leaching process led to an increment of ~100 m^2/g on surface area, which was then responsible for the high catalytic activity.

PHOTOELECTROCHEMICAL WATER OXIDATION BY COBALT-OXIDE-BASED CATALYSTS

Photoelectrochemical (PEC) water splitting using semiconductor materials has attracted considerable attention due to their potential in utilizing solar energy in the past decades.[8,112,113] The principle of PEC water splitting is illustrated in Figure 12. The overall process consists of three steps: (1) Absorption of photons and excitation of semiconductors to generate electron−hole pairs. (2) Migration of generated electrons/holes to the semiconductor-electrolyte interface. (3) Surface reaction of hydrogen and oxygen evolution.

Although numerous materials have been shown to be capable to split water, the overall efficiency is still far from practical application. The performance is always limited by factors such as band gap and band positions of the semiconductors, charge separation and recombination during migration, the slow kinetics of surface reaction, among others.[7,114,115] Because overall water splitting is a thermodynamically uphill reaction which involves a four-electron transfer, one of the biggest challenges is to enhance hydrogen evolution and oxygen evolution half reactions. Cocatalysts loaded on the surface of semiconductors have been proven to be able to facilitate photocatalytic reactions by accommodating excited electrons/holes and promoting redox reaction kinetics.[116] As shown in Figure 13, on the photoanodes in PEC cells, overpotential is

dx.doi.org/10.1021/cs500713d | ACS Catal. 2014, 4, 3701−3714

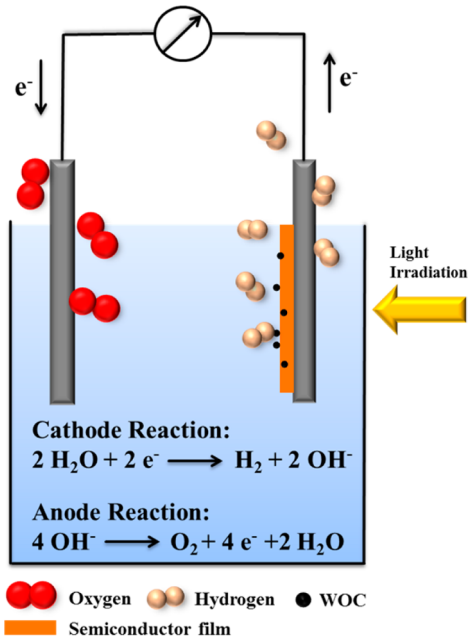

Figure 12. Schematic illustration of photoelectrochemical water oxidation. The semiconductor is first excited by light irradiation and electron–hole pairs are generated. Under applied electrical bias, electrons move to cathode materials and holes are transferred to water oxidation cocatalyst where the water oxidation reaction occurs.

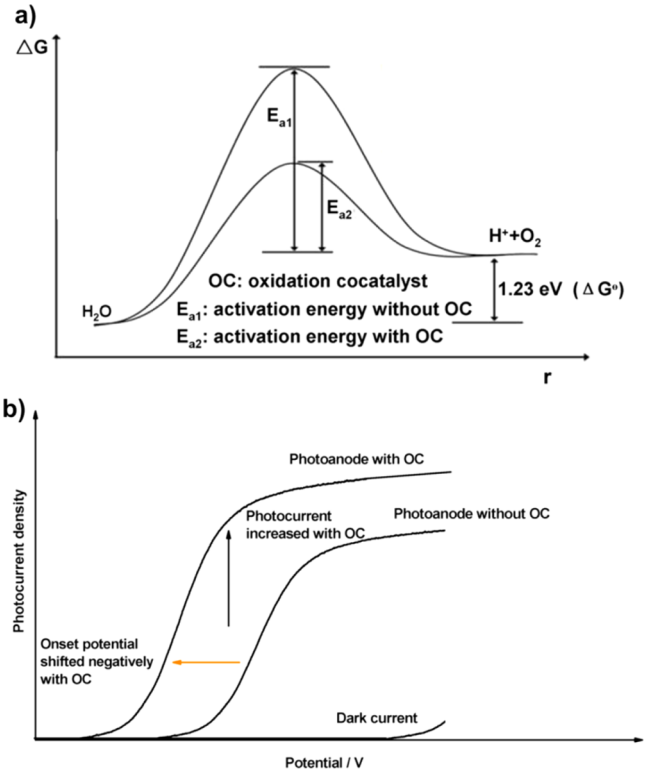

Figure 13. Schematic description of the role of water oxidation cocatalyst in (a) photocatalytic and (b) photoelectrochemical water splitting systems. Adapted with permission from ref 116. Copyright 2013 American Chemical Society.

always necessary to drive the water oxidation reaction due to the activation energy. By decreasing the activation energy (Figure 13a), O_2 evolution cocatalysts can improve the photocurrent and negatively shift the overpotential (Figure 13b) and hence improve the solar and electric energy utilization efficiency. Noble metal oxides such as IrO_x and RuO_x were investigated as conventional water oxidation cocatalysts.[15,117−119] However, non-noble transition metal oxides are emerging as oxygen evolution cocatalysts with advantages such as earth abundance, low cost, and moderate catalytic activity.[120] Among them, cobalt oxide has been intensively integrated with semiconductors such as hematite and tantalum (oxy)-nitride materials. In the following content, we will introduce the major achievements concerning these two systems.

Hematite (α-Fe_2O_3) is a suitable candidate for photoelectrochemical water oxidation due to its natural abundance, stability, and suitable photonic properties. The band gap of hematite is 2.2 eV, which makes it a visible-light-responsive semiconductor.[121−123] Although the valence band is 1 V more positive than thermodynamically required potential for water oxidation, the efficiency is always limited mainly by the charge carriers recombination, hole diffusion issues, and slow kinetics of the oxygen evolution reaction. Regarding the Co-Pi WOC, the Gamelin group found that when cobalt phosphate cocatalyst was electrodeposited on a mesoporous α-Fe_2O_3 photoanode, a 5-fold enhancement of photocurrent and O_2 evolution rate were observed at 1 V vs RHE compared with a bare Fe_2O_3 photoanode in buffered electrolyte (pH = 8).[124,125] Recently, hematite nanorods decorated with Co_3O_4 nanoparticles were reported as effective photoanodes, and in their synthesis, the Fe_2O_3/Co_3O_4 hybrid materials were prepared in one step by high temperature annealing after the hydrothermal growth of hematite nanorods on FTO substrate.[126] The XPS spectra indicated that the Co species were mostly located on the surface and with an optimal amount of Co loading (5%), the overpotential for water oxidation negatively shifted 40 mV, and a photocurrent improvement of 67% was observed at 1.23 V versus RHE under alkaline conditions (pH = 13.6). Incident-photon-to-current efficiencies and oxygen evolution amounts were also compared. Although the advantages of coupling cobalt-based species with hematite photoanodes have been widely confirmed, it has to be mentioned that the original functionality of such modification is still under discussion. The controversies are mainly about whether the photogenerated holes are transferred to and stored by the cobalt oxide layer, or the enhancement is largely due to the formation of heterojunction between photoanode and Co overlayer which contributes to enhance electron depletion in the Fe_2O_3. In the latter case CoO_x is playing a noncatalytic role.[127−130]

Another attractive semiconductor candidate utilized in PEC water oxidation is tantalum (oxy)-nitride-based materials.[131−134] Similar to hematite, the narrow band gap of such materials ensures the absorption of visible light, and the band positions of the conduction band and valence band are suitable for hydrogen and oxygen evolutions, respectively.[135] However, the efficiency is still low and the stability of nitride-based materials suffers from self-oxidative deactivation due to the accumulation of photogenerated holes on the surface. The facile fabrication of TaON and Ta_3N_5 photoanodes by electrophoretic deposition (EPD) was first introduced by Abe/Domen.[136] After that, IrO_2 was employed as cocatalyst to enhance the activity and at the same time to maintain the photoanode stability at Na_2SO_4 electrolyte (pH = 6).[39] Later on from the same group, CoO_x nanoparticles were deposited on as-prepared TaON particles by a simple impregnation–calcination method prior to photoanode preparation, and they

dx.doi.org/10.1021/cs500713d | ACS Catal. 2014, 4, 3701−3714

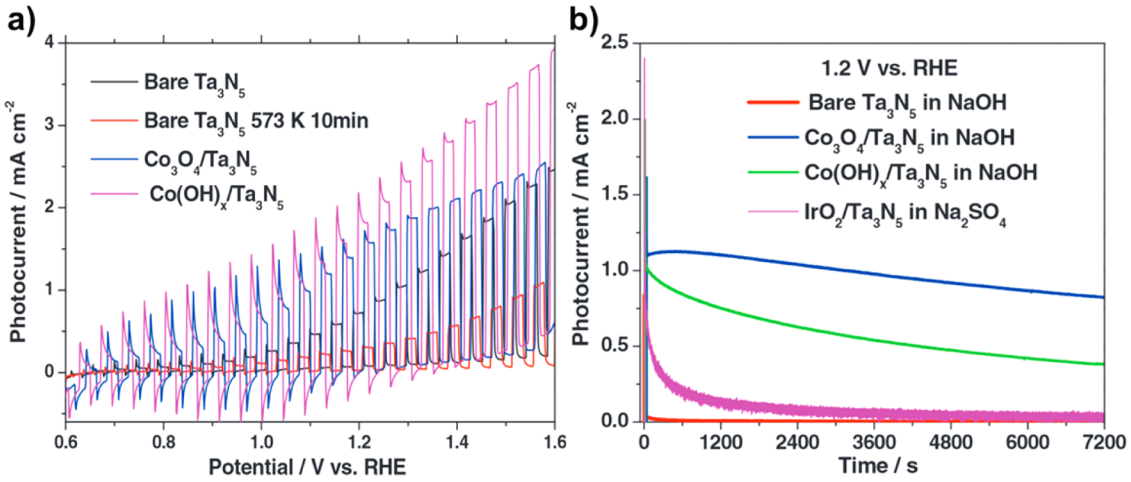

Figure 14. (a) Photocurrent densities of $Co(OH)_x/Ta_3N_5$, Co_3O_4/Ta_3N_5 and bare Ta_3N_5 photoanodes under visible light irradiation (electrolyte: 1 M NaOH). (b) Stability test measured at 1.2 V vs RHE under visible light irradiation. $Co(OH)_x/Ta_3N_5$, Co_3O_4/Ta_3N_5 and bare Ta_3N_5 were measured in 1 M NaOH solution and IrO_2/Ta_3N_5 was measured in 0.5 M Na_2SO_4 soltuion (pH = 6.5). Reprinted with permission from ref 138. Copyright 2012 Wiley-VCH Verlag GmbH & Co. KGaA, Weinheim.

were further reduced in NH_3 stream (XPS spectra indicated that prepared CoO_x/TaON electrodes predominantly contains Co^{2+} species). The photocurrent measurements showed that in the time range of 60 min, the performance of CoO_x-modified TaON photoanode remained stable at 1.07 V versus RHE at Na_2SO_4 solution (pH = 8) under visible light irradiation. More surprisingly, a higher photocurrent was observed compared to IrO_x/TaON electrode.[137] Although a direct comparison was not feasible here because the preparation procedures were not identical, it still demonstrated the superiority of utilizing cobalt-oxide-based materials as low-cost water oxidation cocatalysts. In another work where Ta_3N_5 photoanodes were modified with a $Co(OH)_x$ layer and Co_3O_4 nanoparticles, better performance relative to bare Ta_3N_5 electrodes were observed as well, and the photocurrent curves at 1.2 V vs RHE showed substantial enhancement in the photoanode stability (electrolyte pH = 13.6), as can be seen from Figure 14.[138] Similar work was also conducted by the Bard group in which Co_3O_4 nanoparticles were deposited on Ta_3N_5 nanotube arrays.[139] Moreover, it was demonstrated that a cobalt bilayer (Co_3O_4/Co(II)) catalyst decorated Ta_3N_5 nanorod exhibited substantial enhancement on photocurrent and long-term stability compared with single Co_3O_4-modified photoanodes. EIS (electrochemical impedance spectroscopy) measurements implied that decoration with Co_3O_4/Co(II) bilayer catalysts significantly enhanced the electron mobility by reducing the electron−hole pairs recombination.[140]

Besides the above-mentioned semiconductors, other materials such as TiO_2 nanosheets, porous $LaTiO_2N$, and $BaTaO_2N$ were also investigated with CoO_x being water oxidation cocatalyst.[141−143] Very recently, a photoanode consisting of a novel molecular semiconductor and CoO_x is reported by Finke group. By photodepositing CoO_x cocatalyst on a single-layer organic semiconductor thin film, the device is able to oxidize water under visible light with an internal quantum efficiency of ∼1%.[144] All these results suggest that CoO_x nanoparticles can be promising substitutes for noble metal oxides as cocatalysts in photo- and photoelectrochemical water splitting.

FUTURE PROSPECTS FOR COBALT-OXIDE-BASED WOC

The design and engineering of materials is likely the most important step for fundamental research in addition to their application in various fields, particularly in catalysis. By considering the sustainable energy requirements of society, new materials and technologies need to be developed in order to solve energy-related matters. Nowadays, solar energy can be effectively transferred to electrical energy. This process is commercialized, and the process costs have been decreased dramatically in the past decade. The main dispute of this process is that the energy cannot be stored. Thus, it is necessary to consider the possibility of transferring solar energy to chemical energy where the energy can be stored as a dense renewable fuel. This can be achieved by artificial photosynthesis; however, suitable catalysts are essential to boost kinetics of water oxidation reaction and enhance efficiency in overall schemes. In this perspective, we have demonstrated the possibility of utilizing cobalt-oxide-based catalysts for water oxidation reaction and applications in electrochemical, photochemical, and photoelectrochemcial approaches are discussed separately. Although a great deal of work has been conducted, there is still room for further improvement.

Key factors such as composition, nanostructure, and support materials are playing important roles on the overall activity of the catalysts. In the case of nanocrystals, shape and exposed crystal planes can have a considerable effect on the catalytic performance due to the different surface atom arrangement and number of dangling bonds.[145] Such investigation concerning the OER activity could be interesting and helpful to material design. Nanosize composite and alloy materials could also be promising to further enhance the activity. Although materials in this concept have been reported, they still lack nanostructure optimization. Apart from oxides, nanostructured oxyhydroxides and hydroxides of transition metals are also demonstrated to be promising candidate for water oxidation. It has been recently reported that nickel−iron oxyhydroxide and nickel hydroxide exhibit superior electrocatalytic activity in basic conditions.[20,23,146,147] Considering the possible phase transformation of cobalt species under bias and the positive effect that the other metal doping may offer, it is of great interest to conduct

dx.doi.org/10.1021/cs500713d | ACS Catal. 2014, 4, 3701−3714

study focusing on the synthesis and catalytic activity of nanostructured cobalt-based (oxy)-hydroxide, in which hydrothermal synthesis pathway may play a critical role.

In terms of ordered mesoporous materials, the pore system, pore volume, and surface curvature of catalysts can be further tailored by synthesis strategy. For example, Co_3O_4 in 1D, 2D, and 3D nanostructures can be easily prepared through the nanocasting approach by utilizing different silica templates. Morphologies with high aspect ratio such as 1D ordered nanowire arrays could be used to overcome the poor hole-transport properties and related slow surface reaction kinetics. The domain size and porosity can be further tuned by the amount of precursor applied in the synthesis. Design and development of novel mesostructured binary and ternary composite oxides might be motivating as well. These factors may have an effect on catalyst performance. Moreover, the rigid framework provided by ordered mesoporous oxides can serve as a platform for further surface modification or phase transformation. This makes it more convenient to survey the activity of a variety of catalysts.

For photoelectrochemical water splitting, apart from extending the absorption band of the semiconductor and reducing electron−hole recombination by material engineering, the integration of cocatalyst with photocatalyst is also a critical aspect. Discovery of more efficient WOCs could have the possibility to protect narrow band gap photocatalysts, such as oxynitrides or oxysulfides, from photocorrosion and achieve overall water splitting. It is also extremely significant to engineer interactions between cocatalysts and semiconductors for higher efficiency and performance. Studies based on binary/ternary transition metal oxides and their combination with high surface area mesostructured semiconductor materials is in process in our research group.

AUTHOR INFORMATION

Corresponding Author

*E-mail: tueysuez@kofo.mpg.de.

Notes

The authors declare no competing financial interest.

DEDICATION

This work is dedicated to the 100 year anniversary of Max-Planck-Institut für Kohlenforschung.

REFERENCES

(1) Faunce, T. A.; Lubitz, W.; Rutherford, A. W.; MacFarlane, D. R.; Moore, G. F.; Yang, P. D.; Nocera, D. G.; Moore, T. A.; Gregory, D. H.; Fukuzumi, S.; Yoon, K. B.; Armstrong, F. A.; Wasielewski, M. R.; Styring, S. *Energy Environ. Sci.* **2013**, *6*, 695−698.
(2) Kudo, A.; Miseki, Y. *Chem. Soc. Rev.* **2009**, *38*, 253−278.
(3) Lewis, N. S.; Nocera, D. G. *Proc. Natl. Acad. Sci. U.S.A.* **2006**, *103*, 15729−15735.
(4) Meyer, T. J. *Acc. Chem. Res.* **1989**, *22*, 163−170.
(5) O'Regan, B.; Gratzel, M. *Nature* **1991**, *353*, 737−740.
(6) Turner, J. A. *Science* **2004**, *305*, 972−974.
(7) Grewe, T.; Meier, K.; Tüysüz, H. *Catal. Today* **2014**, *225*, 142−148.
(8) Van de Krol, R.; Liang, Y. Q.; Schoonman, J. *J. Mater. Chem.* **2008**, *18*, 2311−2320.
(9) Artero, V.; Chavarot-Kerlidou, M.; Fontecave, M. *Angew. Chem., Int. Ed.* **2011**, *50*, 7238−7266.
(10) Bard, A. J.; Fox, M. A. *Acc. Chem. Res.* **1995**, *28*, 141−145.
(11) Nakamura, R.; Frei, H. *J. Am. Chem. Soc.* **2006**, *128*, 10668−10669.
(12) Nakagawa, T.; Bjorge, N. S.; Murray, R. W. *J. Am. Chem. Soc.* **2009**, *131*, 15578−15579.
(13) Nakagawa, T.; Beasley, C. A.; Murray, R. W. *J. Phys. Chem.C* **2009**, *113*, 12958−12961.
(14) Smith, R. D. L.; Sporinova, B.; Fagan, R. D.; Trudel, S.; Berlinguette, C. P. *Chem. Mater.* **2014**, *26*, 1654−1659.
(15) Sato, J.; Saito, N.; Yamada, Y.; Maeda, K.; Takata, T.; Kondo, J. N.; Hara, M.; Kobayashi, H.; Domen, K.; Inoue, Y. *J. Am. Chem. Soc.* **2005**, *127*, 4150−4151.
(16) Harriman, A.; Pickering, I. J.; Thomas, J. M.; Christensen, P. A. *J. Chem. Soc., Faraday Trans. 1* **1988**, *84*, 2795−2806.
(17) Gorlin, Y.; Jaramillo, T. F. *J. Am. Chem. Soc.* **2010**, *132*, 13612−13614.
(18) Jiao, F.; Frei, H. *Chem. Commun.* **2010**, *46*, 2920−2922.
(19) Jiao, F.; Frei, H. *Energy Environ. Sci.* **2010**, *3*, 1018−1027.
(20) Kim, T. W.; Choi, K.-S. *Science* **2014**, *343*, 990−994.
(21) Seabold, J. A.; Choi, K.-S. *J. Am. Chem. Soc.* **2012**, *134*, 2186−2192.
(22) Chemelewski, W. D.; Lee, H.-C.; Lin, J.-F.; Bard, A. J.; Mullins, C. B. *J. Am. Chem. Soc.* **2014**, *136*, 2843−2850.
(23) Gong, M.; Li, Y.; Wang, H.; Liang, Y.; Wu, J. Z.; Zhou, J.; Wang, J.; Regier, T.; Wei, F.; Dai, H. *J. Am. Chem. Soc.* **2013**, *135*, 8452−8455.
(24) Jiao, F.; Frei, H. *Angew. Chem., Int. Ed.* **2009**, *48*, 1841−1844.
(25) Brunschwig, B. S.; Chou, M. H.; Creutz, C.; Ghosh, P.; Sutin, N. *J. Am. Chem. Soc.* **1983**, *105*, 4832−4833.
(26) Ghosh, P. K.; Brunschwig, B. S.; Chou, M.; Creutz, C.; Sutin, N. *J. Am. Chem. Soc.* **1984**, *106*, 4772−4783.
(27) Jun, K.; Takahashi, M.; Suzuki, O.; Fukunaga, T. U.S. Patent 3,399,996, September 3, 1968.
(28) Kanan, M. W.; Nocera, D. G. *Science* **2008**, *321*, 1072−1075.
(29) Kanan, M. W.; Surendranath, Y.; Nocera, D. G. *Chem. Soc. Rev.* **2009**, *38*, 109−114.
(30) Lutterman, D. A.; Surendranath, Y.; Nocera, D. G. *J. Am. Chem. Soc.* **2009**, *131*, 3838−3839.
(31) Surendranath, Y.; Dincă, M.; Nocera, D. G. *J. Am. Chem. Soc.* **2009**, *131*, 2615−2620.
(32) Reece, S. Y.; Hamel, J. A.; Sung, K.; Jarvi, T. D.; Esswein, A. J.; Pijpers, J. J. H.; Nocera, D. G. *Science* **2011**, *334*, 645−648.
(33) Kanan, M. W.; Yano, J.; Surendranath, Y.; Dincă, M.; Yachandra, V. K.; Nocera, D. G. *J. Am. Chem. Soc.* **2010**, *132*, 13692−13701.
(34) McAlpin, J. G.; Surendranath, Y.; Dincă, M.; Stich, T. A.; Stoian, S. A.; Casey, W. H.; Nocera, D. G.; Britt, R. D. *J. Am. Chem. Soc.* **2010**, *132*, 6882−6883.
(35) Stracke, J. J.; Finke, R. G. *ACS Catal.* **2013**, *3*, 1209−1219.
(36) Stracke, J. J.; Finke, R. G. *J. Am. Chem. Soc.* **2011**, *133*, 14872−14875.
(37) Yin, Q.; Tan, J. M.; Besson, C.; Geletii, Y. V.; Musaev, D. G.; Kuznetsov, A. E.; Luo, Z.; Hardcastle, K. I.; Hill, C. L. *Science* **2010**, *328*, 342−345.
(38) Grewe, T.; Deng, X.; Weidenthaler, C.; Schüth, F.; Tüysüz, H. *Chem. Mater.* **2013**, *25*, 4926−4935.
(39) Higashi, M.; Domen, K.; Abe, R. *J. Am. Chem. Soc.* **2012**, *134*, 6968−6971.
(40) Rosen, J.; Hutchings, G. S.; Jiao, F. *J. Am. Chem. Soc.* **2013**, *135*, 4516−4521.
(41) Grewe, T.; Deng, X.; Tüysüz, H. *Chem. Mater.* **2014**, *26*, 3162−3168.
(42) McCrory, C. C. L.; Jung, S.; Peters, J. C.; Jaramillo, T. F. *J. Am. Chem. Soc.* **2013**, *135*, 16977−16987.
(43) Singh, R. N.; Koenig, J. F.; Poillerat, G.; Chartier, P. *J. Electroanal. Chem. Interfacial Electrochem.* **1991**, *314*, 241−257.
(44) Singh, R.-N.; Hamdani, M.; Koenig, J.-F.; Poillerat, G.; Gautier, J.; Chartier, P. *J. Appl. Electrochem.* **1990**, *20*, 442−446.
(45) Hamdani, M.; Koenig, J. F.; Chartier, P. *J. Appl. Electrochem.* **1988**, *18*, 568−576.
(46) Hamdani, M.; Koenig, J. F.; Chartier, P. *J. Appl. Electrochem.* **1988**, *18*, 561−567.

(47) Hamdani, M.; Singh, R. N.; Chartier, P. *Int. J. Electrochem. Science* **2010**, *5*, 556−577.
(48) Yeo, B. S.; Bell, A. T. *J. Am. Chem. Soc.* **2011**, *133*, 5587−5593.
(49) Lu, X.; Ng, Y. H.; Zhao, C. *ChemSusChem* **2014**, *7*, 82−86.
(50) Dau, H.; Limberg, C.; Reier, T.; Risch, M.; Roggan, S.; Strasser, P. *ChemCatChem* **2010**, *2*, 724−761.
(51) Gerken, J. B.; McAlpin, J. G.; Chen, J. Y. C.; Rigsby, M. L.; Casey, W. H.; Britt, R. D.; Stahl, S. S. *J. Am. Chem. Soc.* **2011**, *133*, 14431−14442.
(52) Arico, A. S.; Bruce, P.; Scrosati, B.; Tarascon, J.-M.; van Schalkwijk, W. *Nat. Mater.* **2005**, *4*, 366−377.
(53) Philip, M. *Rep. Prog. Phys.* **2001**, *64*, 297.
(54) Xia, Y.; Yang, P.; Sun, Y.; Wu, Y.; Mayers, B.; Gates, B.; Yin, Y.; Kim, F.; Yan, H. *Adv. Mater.* **2003**, *15*, 353−389.
(55) Tüysüz, H.; Comotti, M.; Schüth, F. *Chem. Commun.* **2008**, *34*, 4022−4024.
(56) Grass, M. E.; Rioux, R. M.; Somorjai, G. A. *Catal. Lett.* **2009**, *128*, 1−8.
(57) Lu, A.-H.; Nitz, J.-J.; Comotti, M.; Weidenthaler, C.; Schlichte, K.; Lehmann, C. W.; Terasaki, O.; Schüth, F. *J. Am. Chem. Soc.* **2010**, *132*, 14152−14162.
(58) Yuming, D.; Kun, H.; Lin, Y.; Aimin, Z. *Nanotechnology* **2007**, *18*, 435602.
(59) Esswein, A. J.; McMurdo, M. J.; Ross, P. N.; Bell, A. T.; Tilley, T. D. *J. Phys. Chem. C* **2009**, *113*, 15068−15072.
(60) Chou, N. H.; Ross, P. N.; Bell, A. T.; Tilley, T. D. *ChemSusChem* **2011**, *4*, 1566−1569.
(61) Blakemore, J. D.; Gray, H. B.; Winkler, J. R.; Müller, A. M. *ACS Catal.* **2013**, *3*, 2497−2500.
(62) Geim, A. K.; Novoselov, K. S. *Nat. Mater.* **2007**, *6*, 183−191.
(63) Guo, S.; Dong, S. *Chem. Soc. Rev.* **2011**, *40*, 2644−2672.
(64) Kamat, P. V. *J. Phys. Chem. Lett.* **2011**, *2*, 242−251.
(65) Liu, M.; Zhang, R.; Chen, W. *Chem. Rev.* **2014**, *114*, 5117−5160.
(66) Sun, Y.; Wu, Q.; Shi, G. *Energy. Environ. Sci.* **2011**, *4*, 1113−1132.
(67) Xiang, Q.; Yu, J.; Jaroniec, M. *Chem. Soc. Rev.* **2012**, *41*, 782−796.
(68) Liang, Y. Y.; Li, Y. G.; Wang, H. L.; Zhou, J. G.; Wang, J.; Regier, T.; Dai, H. J. *Nat. Mater.* **2011**, *10*, 780−786.
(69) Wu, J.; Xue, Y.; Yan, X.; Yan, W.; Cheng, Q.; Xie, Y. *Nano Res.* **2012**, *5*, 521−530.
(70) Ciesla, U.; Schüth, F. *Microporous Mesoporous Mater.* **1999**, *27*, 131−149.
(71) Taguchi, A.; Schüth, F. O. *Microporous Mesoporous Mater.* **2005**, *77*, 1−45.
(72) Tüysüz, H.; Schüth, F. *Adv. Catal.* **2012**, *55*, 127−239.
(73) Schmidt, W. *ChemCatChem* **2009**, *1*, 53−67.
(74) Lu, A. H.; Schüth, F. *Adv. Mater.* **2006**, *18*, 1793−1805.
(75) Gu, D.; Schüth, F. *Chem. Soc. Rev.* **2014**, *43*, 313−344.
(76) Shi, Y.; Wan, Y.; Zhao, D. *Chem. Soc. Rev.* **2011**, *40*, 3854−3878.
(77) Tiemann, M. *Chem. Mater.* **2008**, *20*, 961−971.
(78) Yen, H.; Seo, Y.; Guillet-Nicolas, R.; Kaliaguine, S.; Kleitz, F. *Chem. Commun.* **2011**, *47*, 10473−10475.
(79) Ismail, A. A.; Bahnemann, D. W.; Robben, L.; Yarovyi, V.; Wark, M. *Chem. Mater.* **2010**, *22*, 108−116.
(80) Benitez, M. J.; Petracic, O.; Salabas, E. L.; Radu, F.; Tüysüz, H.; Schüth, F.; Zabel, H. *Phys. Rev. Lett.* **2008**, *101*, 097206.
(81) Lu, A. H.; Tüysüz, H.; Schüth, F. *Microporous Mesoporous Mater.* **2008**, *111*, 117−123.
(82) Tüysüz, H.; Lehmann, C. W.; Bongard, H.; Tesche, B.; Schmidt, R.; Schüth, F. *J. Am. Chem. Soc.* **2008**, *130*, 11510−11517.
(83) Tüysüz, H.; Liu, Y.; Weidenthaler, C.; Schüth, F. *J. Am. Chem. Soc.* **2008**, *130*, 14108−14110.
(84) Tüysüz, H.; Salabas, E. L.; Weidenthaler, C.; Schüth, F. *J. Am. Chem. Soc.* **2008**, *130*, 280−287.
(85) Benitez, M. J.; Petracic, O.; Tüysüz, H.; Schüth, F.; Zabel, H. *Europhys. Lett.* **2009**, *88*, 27004.
(86) Tüysüz, H.; Galilea, J. L.; Schüth, F. *Catal. Lett.* **2009**, *131*, 49−53.
(87) Benitez, M. J.; Petracic, O.; Tüysüz, H.; Schüth, F.; Zabel, H. *Phys. Rev. B* **2011**, *83*, 134424 .
(88) Tüysüz, H.; Salabas, E. L.; Bill, E.; Bongard, H.; Spliethoff, B.; Lehmann, C. W.; Schüth, F. *Chem. Mater.* **2012**, *24*, 2493−2500.
(89) Tüysüz, H.; Weidenthaler, C.; Grewe, T.; Salabas, E. L.; Romero, M. J. B.; Schüth, F. *Inorg. Chem.* **2012**, *51*, 11745−11752.
(90) Tüysüz, H.; Weidenthaler, C.; Schüth, F. *Chem.—Eur. J.* **2012**, *18*, 5080−5086.
(91) Tüysüz, H.; Hwang, Y.; Khan, S.; Asiri, A.; Yang, P. *Nano Res.* **2013**, *6*, 47−54.
(92) Sa, Y. J.; Kwon, K.; Cheon, J. Y.; Kleitz, F.; Joo, S. H. *J. Mater. Chem. A* **2013**, *1*, 9992−10001.
(93) Liu, X.; Wang, A.; Wang, X.; Mou, C.-Y.; Zhang, T. *Chem. Commun.* **2008**, 3187−3189.
(94) Simonsen, S. B.; Chakraborty, D.; Chorkendorff, I.; Dahl, S. *Appl. Catal., A* **2012**, *447*, 22−31.
(95) Sarina, S.; Zhu, H. Y.; Jaatinen, E.; Xiao, Q.; Liu, H. W.; Jia, J. F.; Chen, C.; Zhao, J. *J. Am. Chem. Soc.* **2013**, *135*, 5793−5801.
(96) Rumplecker, A.; Kleitz, F.; Salabas, E.-L.; Schüth, F. *Chem. Mater.* **2007**, *19*, 485−496.
(97) Jiao, F.; Hill, A. H.; Harrison, A.; Berko, A.; Chadwick, A. V.; Bruce, P. G. *J. Am. Chem. Soc.* **2008**, *130*, 5262−5266.
(98) Doi, Y.; Takai, A.; Sakamoto, Y.; Terasaki, O.; Yamauchi, Y.; Kuroda, K. *Chem. Commun.* **2010**, *46*, 6365−6367.
(99) Merrill, M. D.; Dougherty, R. C. *J. Phys. Chem. C* **2008**, *112*, 3655−3666.
(100) Ho, J.; Piron, D. *J. Appl. Electrochem.* **1996**, *26*, 515−521.
(101) Smith, R. D. L.; Prévot, M. S.; Fagan, R. D.; Zhang, Z.; Sedach, P. A.; Siu, M. K. J.; Trudel, S.; Berlinguette, C. P. *Science* **2013**, *340*, 60−63.
(102) Smith, R. D. L.; Prévot, M. S.; Fagan, R. D.; Trudel, S.; Berlinguette, C. P. *J. Am. Chem. Soc.* **2013**, *135*, 11580−11586.
(103) Kiwi, J.; Grätzel, M. *Angew. Chem., Int. Ed. Engl.* **1978**, *17*, 860−861.
(104) Robinson, D. M.; Go, Y. B.; Mui, M.; Gardner, G.; Zhang, Z. J.; Mastrogiovanni, D.; Garfunkel, E.; Li, J.; Greenblatt, M.; Dismukes, G. C. *J. Am. Chem. Soc.* **2013**, *135*, 3494−3501.
(105) Agiral, A.; Soo, H. S.; Frei, H. *Chem. Mater.* **2013**, *25*, 2264−2273.
(106) Soo, H. S.; Agiral, A.; Bachmeier, A.; Frei, H. *J. Am. Chem. Soc.* **2012**, *134*, 17104−17116.
(107) Zhang, M.; de Respinis, M.; Frei, H. *Nat. Chem.* **2014**, *6*, 362−367.
(108) Yusuf, S.; Jiao, F. *ACS Catal.* **2012**, *2*, 2753−2760.
(109) Grzelczak, M.; Zhang, J.; Pfrommer, J.; Hartmann, J.; Driess, M.; Antonietti, M.; Wang, X. *ACS Catal.* **2013**, *3*, 383−388.
(110) Zhang, Y.; Rosen, J.; Hutchings, G. S.; Jiao, F. *Catal. Today* **2013**, *225*, 171−176.
(111) Rosen, J.; Hutchings, G. S.; Jiao, F. *J. Catal.* **2014**, *310*, 2−9.
(112) Gratzel, M. *Nature* **2001**, *414*, 338−344.
(113) Tüysüz, H.; Chan, C. K. *Nano Energy* **2013**, *2*, 116−123.
(114) Chen, X.; Shen, S.; Guo, L.; Mao, S. S. *Chem. Rev.* **2010**, *110*, 6503−6570.
(115) Walter, M. G.; Warren, E. L.; McKone, J. R.; Boettcher, S. W.; Mi, Q.; Santori, E. A.; Lewis, N. S. *Chem. Rev.* **2010**, *110*, 6446−6473.
(116) Yang, J.; Wang, D.; Han, H.; Li, C. *Acc. Chem. Res.* **2013**, *46*, 1900−1909.
(117) Maeda, K.; Teramura, K.; Masuda, H.; Takata, T.; Saito, N.; Inoue, Y.; Domen, K. *J. Phys. Chem. B* **2006**, *110*, 13107−13112.
(118) Sayama, K.; Mukasa, K.; Abe, R.; Abe, Y.; Arakawa, H. *J. Photochem. Photobiol., A* **2002**, *148*, 71−77.
(119) Youngblood, W. J.; Lee, S.-H. A.; Maeda, K.; Mallouk, T. E. *Acc. Chem. Res.* **2009**, *42*, 1966−1973.
(120) Maeda, K.; Xiong, A.; Yoshinaga, T.; Ikeda, T.; Sakamoto, N.; Hisatomi, T.; Takashima, M.; Lu, D.; Kanehara, M.; Setoyama, T.; Teranishi, T.; Domen, K. *Angew. Chem.* **2010**, *122*, 4190−4193.

(121) Lin, Y.; Yuan, G.; Sheehan, S.; Zhou, S.; Wang, D. *Energy. Environ. Sci.* **2011**, *4*, 4862−4869.
(122) Sivula, K.; Le Formal, F.; Grätzel, M. *ChemSusChem* **2011**, *4*, 432−449.
(123) Tilley, S. D.; Cornuz, M.; Sivula, K.; Grätzel, M. *Angew. Chem.* **2010**, *122*, 6549−6552.
(124) Zhong, D. K.; Gamelin, D. R. *J. Am. Chem. Soc.* **2010**, *132*, 4202−4207.
(125) Zhong, D. K.; Sun, J.; Inumaru, H.; Gamelin, D. R. *J. Am. Chem. Soc.* **2009**, *131*, 6086−6087.
(126) Xi, L.; Tran, P. D.; Chiam, S. Y.; Bassi, P. S.; Mak, W. F.; Mulmudi, H. K.; Batabyal, S. K.; Barber, J.; Loo, J. S. C.; Wong, L. H. *J. Phys. Chem. C* **2012**, *116*, 13884−13889.
(127) Barroso, M.; Cowan, A. J.; Pendlebury, S. R.; Grätzel, M.; Klug, D. R.; Durrant, J. R. *J. Am. Chem. Soc.* **2011**, *133*, 14868−14871.
(128) Barroso, M.; Mesa, C. A.; Pendlebury, S. R.; Cowan, A. J.; Hisatomi, T.; Sivula, K.; Grätzel, M.; Klug, D. R.; Durrant, J. R. *Proc. Natl. Acad. Sci. U.S.A.* **2012**, *109*, 15640−15645.
(129) Klahr, B.; Gimenez, S.; Fabregat-Santiago, F.; Bisquert, J.; Hamann, T. W. *J. Am. Chem. Soc.* **2012**, *134*, 16693−16700.
(130) Gamelin, D. R. *Nat. Chem.* **2012**, *4*, 965−967.
(131) Hara, M.; Hitoki, G.; Takata, T.; Kondo, J. N.; Kobayashi, H.; Domen, K. *Catal. Today* **2003**, *78*, 555−560.
(132) Hitoki, G.; Takata, T.; Kondo, J. N.; Hara, M.; Kobayashi, H.; Domen, K. *Chem. Commun.* **2002**, 1698−1699.
(133) Maeda, K.; Domen, K. *J. Phys. Chem. Lett.* **2010**, *1*, 2655−2661.
(134) Cong, Y.; Park, H. S.; Dang, H. X.; Fan, F.-R. F.; Bard, A. J.; Mullins, C. B. *Chem. Mater.* **2012**, *24*, 579−586.
(135) Chun, W.-J.; Ishikawa, A.; Fujisawa, H.; Takata, T.; Kondo, J. N.; Hara, M.; Kawai, M.; Matsumoto, Y.; Domen, K. *J. Phys. Chem. B* **2003**, *107*, 1798−1803.
(136) Abe, R.; Higashi, M.; Domen, K. *J. Am. Chem. Soc.* **2010**, *132*, 11828−11829.
(137) Higashi, M.; Domen, K.; Abe, R. *Energy. Environ. Sci.* **2011**, *4*, 4138−4147.
(138) Liao, M.; Feng, J.; Luo, W.; Wang, Z.; Zhang, J.; Li, Z.; Yu, T.; Zou, Z. *Adv. Funct. Mater.* **2012**, *22*, 3066−3074.
(139) Cong, Y.; Park, H. S.; Wang, S.; Dang, H. X.; Fan, F.-R. F.; Mullins, C. B.; Bard, A. J. *J. Phys. Chem. C* **2012**, *116*, 14541−14550.
(140) Hou, J.; Wang, Z.; Yang, C.; Cheng, H.; Jiao, S.; Zhu, H. *Energy. Environ. Sci.* **2013**, *6*, 3322−3330.
(141) Zhang, F.; Yamakata, A.; Maeda, K.; Moriya, Y.; Takata, T.; Kubota, J.; Teshima, K.; Oishi, S.; Domen, K. *J. Am. Chem. Soc.* **2012**, *134*, 8348−8351.
(142) Higashi, M.; Domen, K.; Abe, R. *J. Am. Chem. Soc.* **2013**, *135*, 10238−10241.
(143) Liu, L.; Ji, Z.; Zou, W.; Gu, X.; Deng, Y.; Gao, F.; Tang, C.; Dong, L. *ACS Catal.* **2013**, *3*, 2052−2061.
(144) Kirner, J. T.; Stracke, J. J.; Gregg, B. A.; Finke, R. G. *ACS Appl. Mater. Interfaces* **2014**, *6*, 13367−13377.
(145) Hu, L.; Peng, Q.; Li, Y. *J. Am. Chem. Soc.* **2008**, *130*, 16136−16137.
(146) Gao, M.; Sheng, W.; Zhuang, Z.; Fang, Q.; Gu, S.; Jiang, J.; Yan, Y. *J. Am. Chem. Soc.* **2014**, *136*, 7077−7084.
(147) Trotochaud, L.; Young, S. L.; Ranney, J. K.; Boettcher, S. W. *J. Am. Chem. Soc.* **2014**, *136*, 6744−6753.